applied sciences

MDPI

Article

Influence of Low Temperature on Nitrate Removal Efficiency in Woodchip Denitrifying Bioreactors: Implications for Bioreactor Design

Jurgita Dabulytė-Bagdonavičienė [1], Feliksas Ivanauskas [2] and Arvydas Povilaitis [3,*]

[1] Department of Applied Mathematics, Kaunas University of Technology, Studentu Str. 50, LT-51368 Kaunas, Lithuania; jurgita.dabulyte@ktu.lt
[2] Institute of Computer Science, Vilnius University, Naugarduko Str. 24, LT-03225 Vilnius, Lithuania; feliksas.ivanauskas@mif.vu.lt
[3] Water Engineering Department, Vytautas Magnus University, K. Donelaičio Str. 58, LT-44248 Kaunas, Lithuania
* Correspondence: arvydas.povilaitis@vdu.lt

Abstract

In this study, a mathematical model based on nonlinear differential equations was developed to describe nitrate (NO_3^-) removal in a woodchip denitrification bioreactor treating tile drainage water. The model captures temperature-dependent denitrification kinetics and transport processes under variable operating conditions. The model was validated using pilot-scale experimental data collected at different inflow water temperatures. The results indicated a strong temperature dependence of nitrate removal efficiency, with higher performance at elevated temperatures due to increased microbial activity and reaction rates. After validation, numerical simulations using a finite difference scheme were performed to evaluate bioreactor performance under varying hydraulic and geometric conditions. The analysis focused on the effect of bioreactor length, assuming constant width and depth (1.0 m each). Results showed that increasing reactor length enhances NO_3^- removal by extending hydraulic retention time, although the effect becomes nonlinear due to substrate limitation along the flow path. Simulations further demonstrated that a target NO_3^- removal efficiency of approximately 40% can be achieved through different combinations of temperature, bioreactor length, and hydraulic loading, indicating a compensatory relationship between kinetic and design parameters. Overall, this study provides a predictive framework for optimizing bioreactor design and operation, offering practical guidance for improving nitrate removal in agricultural drainage systems.

Keywords: denitrification; woodchip bioreactor; nitrate removal; mathematical modelling

Academic Editors: Dario Savoca and Silvia Orecchio

Received: 2 May 2026
Revised: 27 May 2026
Accepted: 28 May 2026
Published: 1 June 2026

1. Introduction

Modern agriculture relies heavily on the application of mineral fertilizers to optimize plant growth and meet the increasing global demand for food. However, this practice often leads to nutrient losses, particularly in the form of inorganic nitrogen (N), which can leach from soils into surface waters. The presence of tile drainage systems further accelerates this process [1]. Such nutrient enrichment adversely affects aquatic ecosystems by promoting eutrophication, stimulating excessive algal blooms, depleting oxygen, and disrupting ecosystem balance. To mitigate these effects, nutrient inflows must be intercepted before they reach surface waters.

Among promising edge-of-field technologies, woodchip denitrifying bioreactors have been developed to remove nitrate (NO_3^-) from tile drainage water [2,3]. These bioreactors consist of a dug subsurface trench filled with woodchips, through which drainage water is directed. Typically, the trench is lined with an impermeable barrier to prevent bypass flow, and the size and shape of the bioreactor are designed to optimize water retention time, which is one of the critical factors for effective NO_3^- removal [4]. The removal of NO_3^- occurs through enhanced denitrification, during which heterotrophic bacteria under anaerobic conditions use carbon from the woodchips as an electron donor, reducing NO_3^- to gaseous nitrogen while oxidizing the organic carbon [5]. The efficiency of this process is influenced not only by the type and age of woodchips but also by seasonal variations in temperature, flow rate, and nitrate concentration [6,7]. Previous studies [8–10] have reported that such bioreactors can reduce annual NO_3^- loads in drainage water by 32–55%. However, removal efficiency can vary substantially between sites, depending on hydrological conditions and bioreactor maintenance practices. Nevertheless, limited research has focused on how design characteristics influence bioreactor performance. Recent findings [11–15] suggest that appropriate design optimization can enhance microbial activity, improve hydraulic performance, and reduce the carbon-to-nitrogen consumption ratio. Furthermore, the integration of real-time monitoring systems and predictive modelling can further inform adaptive management strategies, allowing adjustments in bioreactor dimensions, substrate selection, and flow regulation to maximize NO_3^- removal while minimizing operational costs [16].

Denitrification, however, is a temperature-dependent process. Consequently, bioreactor performance tends to decline at lower temperatures (below 10 °C), resulting in a reduced NO_3^- removal efficiency [17–20]. This temperature sensitivity is primarily due to the reduced metabolic activity of denitrifying bacteria under cold conditions, which slows the enzymatic reactions responsible for the reduction of nitrate [17]. Seasonal fluctuations in water temperature, combined with low ambient temperatures in temperate climates, significantly limit the effectiveness of bioreactors. Despite the well-established influence of low temperatures on denitrification efficiency in bioreactors, there remains a limited quantitative understanding of how design parameters can mitigate temperature-induced impacts on NO_3^- removal performance. Moreover, only a limited number of studies integrate continuous field monitoring data with mathematical modelling approaches to reliably predict denitrification dynamics under varying environmental and operational conditions. The main limitation of existing mathematical models is that most rely on simplified temperature correction functions and therefore do not adequately represent overall system performance. Limited calibration using long-term field data, together with weak integration of continuous monitoring data, further reduces their predictive reliability under real operational conditions.

By integrating experimental data with mathematical modelling, quantitative insights into the interplay between operational parameters and denitrification dynamics can be derived, thereby enabling evidence-based recommendations for bioreactor optimization. Therefore, this study proposes that adjusting bioreactor length may enhance NO_3^- removal efficiency under low-temperature conditions by compensating for reduced biological activity. In line with this, a mathematical modelling approach is applied to evaluate the effects of inflow water temperature and bioreactor length on NO_3^- removal performance. The computational tool also includes continuous monitoring of water temperature, flow rates, dissolved oxygen (O_2) and NO_3^- concentrations, ensuring that model calibration and validation are based on real measurement data.

The article is structured to provide a detailed assessment of NO_3^- removal in woodchip denitrifying bioreactors under low-temperature conditions and to explore the implica-

tions for bioreactor design. Section 2 describes the experimental and modelling approaches used in the study. The pilot-scale woodchip denitrifying bioreactor setup, its design, operational conditions, measurement procedures, and key physical and chemical parameters used to assess the nitrate removal efficiency are presented in Section 2.1. The mathematical model used to simulate the dynamic behavior of O_2 and NO_3^- over time in the denitrifying woodchip bioreactor described by a coupled system of partial differential equations is presented in Section 2.2. The outcomes of both the field pilot-scale and modelling experiments are presented in Section 3. Evaluation of the precision and validity of the mathematical model, comparing simulated data with experimental measurements, is presented in Section 3.1. The investigation of how variations in reactor length affect nitrate removal performance, with particular attention to low-temperature conditions, is presented in Section 3.2. Finally, Section 4 presents and discusses the main results of the study, focusing on the influence of inflow water temperature and bioreactor design on nitrate removal efficiency. Section 5 provides the main conclusions derived from the study.

2. Materials and Methods

2.1. Pilot-Scale Field Experiment

The data used in this study were derived from the experiment described by Vismontienė and Povilaitis [1], while the mathematical approach, integrating mathematical modelling and PI control and incorporating an extended data record for a more comprehensive analysis, was reported by Nečiporenko et al. [21].

Therefore, only the key methodological aspects of the experimental setup are presented below.

The pilot-scale system design included a cube-shaped plastic denitrification bioreactor (1.0 m^3 volume container), placed underground in a 1.2 m trench (Figure 1). The bioreactor's water supply was sourced from two interconnected plastic water tanks, each with a volume of 1.0 m^3. The container was filled with mixed woodchips, obtained from local raw materials, with an average porosity of 56%. The woodchips primarily consisted of alder (*Alnus glutinosa*) and pine (*Pinus sylvestris*) tree scraps. The particle size distribution of the woodchips was predominantly in the range of 1.1 to 3.0 cm, which accounted for 65% of the cumulative distribution, and the bulk density was 260 kg/m^3. The bioreactor was filled with woodchips to a depth of 1.0 m, and the saturation level was maintained at 0.90 m.

The measurements were conducted under two distinct operational conditions: flowing and non-flowing water. Nitrate (NO_3^-) removal efficiency was evaluated as the difference between the inlet and outlet nitrate concentrations, divided by the inlet concentration. The experiment began on 20 July 2017, and ran until 10 March 2019. The water was supplied to the bioreactor by gravity from the tanks, and the inflow and outflow rates were manually adjusted using valves. Nitrate was continuously fed into the bioreactor via the addition of sodium nitrate ($NaNO_3$) to the water tanks, maintaining NO_3^- concentrations within the range of 28.0 to 132.0 $mg \cdot L^{-1}$, with an average concentration of 66.1 $mg \cdot L^{-1}$. These concentrations were typical of those observed in tile drainage water, with 83% of the measurements falling within this range. Outflow NO_3^- concentrations ranged from 16.0 to 98.0 $mg \cdot L^{-1}$, with an average value of 42.4 $mg \cdot L^{-1}$. As a result, the NO_3^- removal efficiency varied between 17.5% and 73.4%, with an average of 35.6%.

Throughout the study period, the water temperatures at both the inlet and the outlet ranged from 1.8 to 19.4 °C. Inflow pH values ranged from 7.8 to 9.0, while outflow pH values varied from 6.2 to 8.3. The O_2 concentrations at the inlet ranged from 3.2 to 4.4 $mg \cdot L^{-1}$, while at the outlet from 0.0 to 1.3 $mg \cdot L^{-1}$. Measurements were taken at irregular intervals, ranging from 16.43 to 183.3 h, following standardized sampling procedures. A total of 108 records were collected and subsequently used in mathematical simulations.

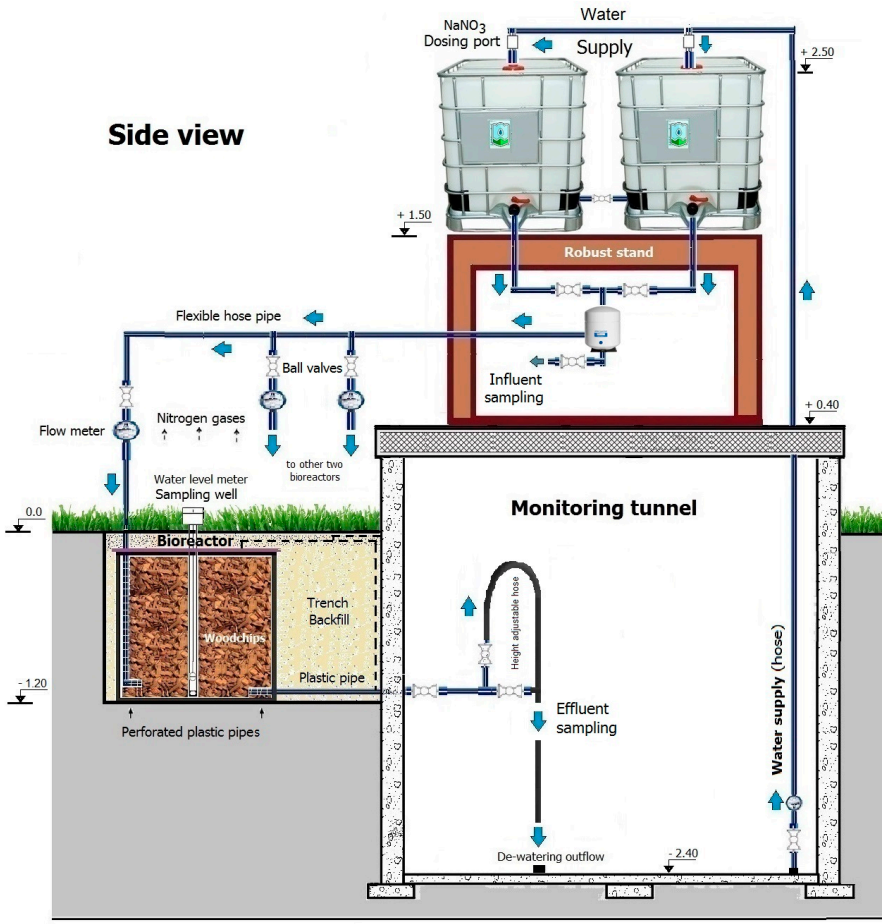

Figure 1. Schematic representation of the pilot-scale woodchip denitrification bioreactor [1].

Nitrate concentrations were measured by spectrometric analysis using a Photometer MD600/MaxDirect system (accuracy ±0.5 mg·L^{-1}; Lovibond®, Dortmund, Germany) with powder reagents. The same equipment was also used to determine nitrite (NO_2^-) and ammonium (NH_4^+), which are not reported herein but may occur in bioreactors under anaerobic conditions. The dissolved oxygen content (accuracy ±1.5%) and water temperatures (accuracy ±0.2 °C) were measured using a portable HI-9142 multimeter (Hanna® Instruments Ltd., Woonsocket, RI, USA), while pH values were recorded using a HI-98136 meter (accuracy ±0.1 pH).

2.2. Modelling Experiment

The distribution of O_2 and NO_3^- concentrations over time in the denitrifying woodchip bioreactor is described by a coupled system of partial differential equations [22]. This system represents the simultaneous physical and biochemical processes occurring within the bioreactor, including advection, diffusion, and microbial substrate consumption. The dynamic behavior of both O_2 and NO_3^- is expressed as follows:

$$\begin{cases} \frac{\partial O}{\partial t} = D\frac{\partial^2 O}{\partial x^2} - v\frac{\partial O}{\partial x} - V_{O,21\,^\circ C}\theta_O^{T-21}\left(\frac{O}{K_O+O}\right), \\ \frac{\partial N}{\partial t} = D\frac{\partial^2 N}{\partial x^2} - v\frac{\partial N}{\partial x} - V_{N,21\,^\circ C}\theta_N^{T-21}\left(\frac{N}{K_N+N}\right)\left(\frac{K_I}{K_I+O}\right), \end{cases} \quad (1)$$

$$x \in [0; a],\ t > 0,$$

where $O(t, x)$ is O_2 concentration (mg L^{-1}), $N(t, x)$ is NO_3^- concentration (mg L^{-1}). The parameter v denotes the porewater velocity (cm h^{-1}), while D is the diffusion coefficient (cm^2 h^{-1}), describing the transport of solutes through the porous woodchip medium. The

kinetic terms are modelled using Monod-type functions, where K_O is O_2 half-saturation constant (mg L^{-1}), K_N is NO_3^- half-saturation constant (mg L^{-1}) and K_I is O_2 inhibition constant (mg L^{-1}), which reflects the suppressing effect of oxygen on the denitrification process. The coefficients $V_{O,21\,^\circ C}$ and $V_{N,21\,^\circ C}$ represent the maximum substrate uptake rates at 21 °C (mg L^{-1} h^{-1}) under aerobic and denitrifying conditions, respectively. The temperature dependence is incorporated through the dimensionless coefficients θ_O and θ_N which adjust the biological reaction rates according to water temperature T (°C). The spatial coordinate x represents the longitudinal distance along the bioreactor (cm), a is the bioreactor length (cm), and t is time (h).

Since the goal is to simulate the temporal variation of NO_3^- and O_2 concentrations within the bioreactor, the initial conditions ($t = 0$) for both parameters are defined as uniform throughout the medium:

$$O(0, x) = O_0, \tag{2}$$

$$N(0, x) = N_0, \tag{3}$$

where O_0 is the initial O_2 concentration (mg L^{-1}), N_0 is the initial NO_3^- concentration (mg L^{-1}).

At the inlet of the bioreactor ($x = 0$), Dirichlet-type boundary conditions ($t > 0$) were applied, assuming constant inflow concentrations of O_2 and NO_3^-. These conditions represent a steady and well-mixed influent entering the system:

$$O(t, x)|_{x=0} = O_{in}, \tag{4}$$

$$N(t, x)|_{x=0} = N_{in}, \tag{5}$$

where O_{in} and N_{in} denote O_2 and NO_3^- concentrations in the inlet water (mg L^{-1}), respectively.

At the outlet ($x = a$), Neumann-type (zero-gradient) boundary conditions ($t > 0$) were employed to describe advection-dominated transport, implying that diffusive fluxes of both O_2 and NO_3^- are negligible at the exit of the bioreactor:

$$\left.\frac{\partial O}{\partial x}\right|_{x=a} = 0, \tag{6}$$

$$\left.\frac{\partial N}{\partial x}\right|_{x=a} = 0. \tag{7}$$

The system of partial differential Equation (1), supplemented with the initial conditions (2)–(3) and the boundary conditions (4)–(7), was solved numerically using the finite-difference method based on an explicit scheme [23]. To perform the numerical calculations, a dedicated computational tool was developed in MATLAB (The MathWorks, Natick, MA, USA, MATLAB R2025b). The developed program enables discretization of both spatial and temporal domains, automatically constructs the finite-difference mesh, and iteratively updates concentration values at each time step according to the governing equations. The spatial and temporal discretization was performed using a uniform grid consisting of 100 spatial nodes over a reactor length of 100 cm, resulting in a spatial step size of $\Delta x = 1$ cm, while the time step was set to $\Delta t = 0.001$. These discretization parameters were selected to ensure numerical stability, accuracy, and sufficient resolution of concentration gradients. Numerical stability was ensured by satisfying the Courant–Friedrichs–Lewy (CFL) condition and further verified through time-step reduction tests, which confirmed that further decreases in Δt did not lead to any significant changes in the model output. In addition, a grid-independence test was performed by comparing model outputs using

refined spatial discretizations, confirming that further mesh refinement did not lead to significant changes in the simulated results.

The explicit finite-difference scheme was selected due to its computational simplicity, straightforward implementation, and suitability for resolving transient concentration dynamics in one-dimensional reactive transport systems. Although implicit schemes generally provide improved numerical stability for stiff reactive systems, the selected discretization parameters ensured stable and accurate solutions within the investigated operating conditions.

The implemented algorithm provides the flexibility to modify model parameters, such as diffusion coefficients, porewater velocity, and temperature-dependent kinetic coefficients. This approach enables the simulation of different operational scenarios. The numerical framework described above was used to generate model outputs that were subsequently compared with experimental data in order to evaluate model performance.

3. Results

3.1. Comparison of Measured and Simulation Results

Field measurements were conducted under varying water temperature conditions at the inlet and outlet of the bioreactor in order to investigate the effect of temperature on NO_3^- removal efficiency. The temperature regime was intentionally altered so that in some experiments the inlet water temperature was lower than the outlet temperature, while in others it was the opposite. Of a total 106 measurements, 59 tests lasting between 50 and 190 min were selected for detailed modelling analysis. In these selected cases, the temperature of the outlet water was lower than at the inlet, allowing for a more comprehensive evaluation of temperature-dependent processes. The measured NO_3^- concentrations at the bioreactor inlet and outlet over time are presented in Figure 2.

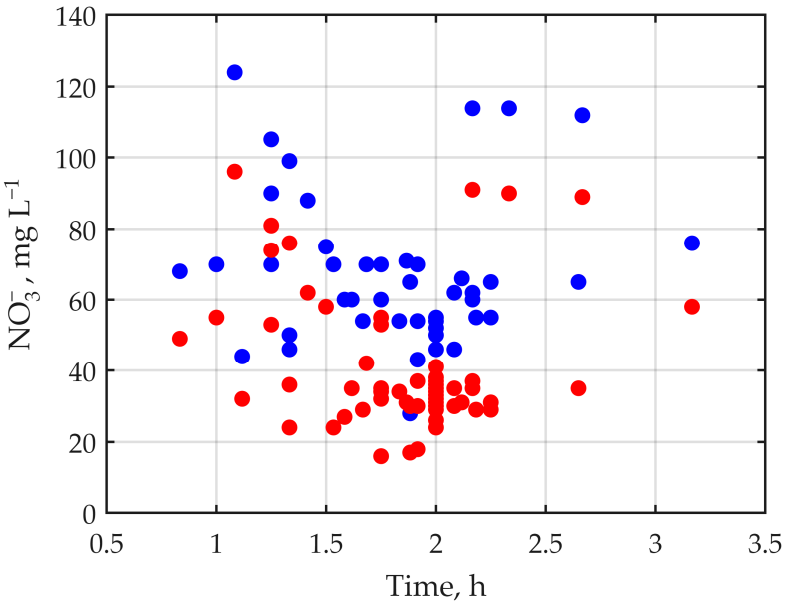

Figure 2. NO_3^- concentrations, recorded during 59 measurements at the inlet (blue dots) and at the outlet (red dots) of the bioreactor.

Based on these measurements, the NO_3^- removal efficiency (%) was calculated. As shown in Figure 3, when the experiments were performed at low inflow water temperatures (6–12 °C), the NO_3^- removal efficiency did not exceed 30%. However, at higher temperatures (14–19 °C), the bioreactor achieved significantly greater NO_3^- removal—up to 73% in some cases, with an average efficiency of approximately 43%. This clearly indicates a strong temperature dependence of the denitrification process.

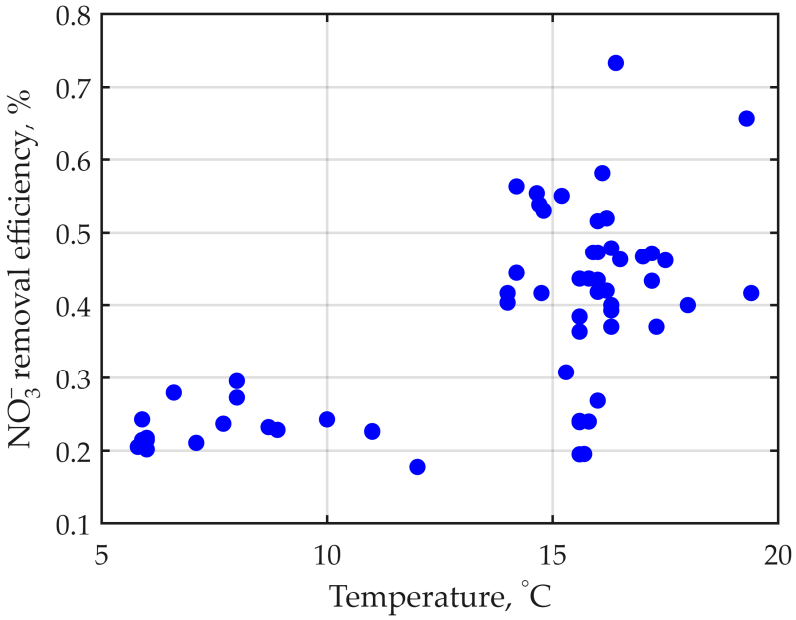

Figure 3. The NO_3^- removal efficiency when performing experiments at different inflow water temperatures.

To compare the experimental and modelling results, 13 representative experimental measurements were selected across the full range of water temperatures (6.0–19.4 °C) to ensure diversity of temperature conditions. In the total dataset of 59 measurements, the initial temperature varied between 5.8 °C and 19.4 °C.

The parameters used for numerical simulations are listed in Table 1. Since several parameters of the mathematical model were unknown or difficult to determine directly, their initial values were adopted from the literature [22] and subsequently refined through a parameter estimation procedure.

Table 1. The values used for the simulations.

Parameters	Symbols	Units	Values
Initial dissolved oxygen concentration	O_0	[mg L^{-1}]	3.25
Initial nitrate concentration	N_0	[mg L^{-1}]	28
Concentration of dissolved oxygen at the inlet	O_{in}	[mg L^{-1}]	3.25
Nitrate concentration at the inlet	N_{in}	[mg L^{-1}]	28
Porewater velocity	v	[cm h^{-1}]	1.4–8.2
Diffusion coefficient	D	[cm^2 h^{-1}]	3.4–24.1
Length of the bioreactor	a	[cm]	100
Dissolved oxygen half-saturation constant	K_O	[mg L^{-1}]	0.1 [22]
Nitrate half-saturation constant	K_N	[mg L^{-1}]	0.05 [22]
Dissolved oxygen inhibition constant	K_I	[mg L^{-1}]	0.1 [22]
Maximum uptake rate of dissolved oxygen under aerobic conditions at 21 °C	$V_{O,21\,°C}$	[mg L^{-1} h^{-1}]	16.54 [22]
Maximum uptake rate of nitrate during denitrification at 21 °C	$V_{N,21\,°C}$	[mg L^{-1} h^{-1}]	0.66 [22]
Temperature coefficient for aerobic respiration	θ_O	[−]	1.2 [22]
Temperature coefficient for denitrification	θ_N	[−]	1.15 [22]
Water temperature	T	[°C]	6–19

The model calibration was formulated as an inverse problem, where the aim was to estimate the unknown model parameters from experimental observations of NO_3^- removal efficiency. In this framework, the mathematical model can be interpreted as a nonlinear mapping:

$$E^{\text{model}} = \mathcal{F}(p, T, \mathrm{x}), \tag{8}$$

where E^{model} denotes the simulated NO_3^- removal efficiency, p is the vector of unknown model parameters, T represents temperature, and x denotes other system variables.

The inverse problem consists of determining the parameter vector p such that the model output best fits the experimental data $E^{\text{experiment}}$. This was achieved by solving the following optimization problem:

$$\min_p \sqrt{\frac{1}{n}\sum_{i=1}^{n}\left(E_i^{\text{model}}(p) - E_i^{\text{experiment}}\right)^2}, \tag{9}$$

where $p = \{a, v, \theta_O, \theta_N, V_{O,21\,^\circ C}, V_{N,21\,^\circ C}\}$.

It should be emphasized that the parameters included in vector p represent a combination of physical, transport-related, and kinetic coefficients used within the modelling framework. The values reported in Table 1 correspond to initial literature-based estimates applied for model initialization and are not treated as fixed constants during the calibration procedure. Within the inverse modelling framework, the temperature-dependent kinetic parameters (θ_O, θ_N and $V_{N,21\,^\circ C}$) were identified as the most sensitive with respect to variations in temperature and model structure. Consequently, these parameters were subject to recalibration in order to reproduce the experimentally observed NO_3^- removal dynamics across different thermal regimes. The resulting calibrated values should therefore be interpreted as effective, system-specific representations of process kinetics rather than universal physical constants.

Due to the nonlinear nature of the model and potential parameter interdependencies, the inverse problem can be considered moderately ill-posed, requiring careful parameter initialization and iterative refinement. Transport-related parameters were constrained using experimentally measured hydraulic characteristics of the pilot-scale bioreactor, while parameter estimation was performed using a nonlinear least-squares optimization framework implemented in MATLAB. The algorithm iteratively minimized the objective function by updating the parameter vector p until convergence was achieved. Convergence was assumed when the relative change in the objective function (RMSE) between successive iterations fell below a predefined threshold of 10^{-6}, a value commonly used in MATLAB-based nonlinear least-squares optimization to ensure numerical stability and convergence robustness, and no further significant improvement in model fit was observed.

The comparison between simulated and measured NO_3^- removal efficiencies is presented in Figure 4 using a 1:1 parity plot. The relative deviation between model predictions and experimental data remained below 3% for the selected representative dataset, indicating a high level of agreement within the range of observed experimental variability.

A quantitative validation of the model performance was carried out using several statistical error metrics. The results demonstrate strong agreement between simulated and measured values, as reflected by the statistical metrics. The coefficient of determination was very high ($R^2 = 0.9983$), indicating good model performance within the investigated range. However, such a very high coefficient of determination should be interpreted with caution, as it may also indicate a potential risk of overfitting, particularly in models calibrated on limited datasets. This concern is particularly relevant given the limited size of the validation dataset, which may lead to an optimistic estimation of model performance.

The mean error (ME = 0.041%) was close to zero, suggesting the absence of systematic bias. The mean absolute error (MAE = 0.304%) and the root mean square error (RMSE = 0.375%) confirm that absolute deviations are small and uniformly distributed.

The relative error analysis confirms low deviations between simulated and measured values. The mean absolute percentage error (MAPE = 1.049%) remained low, while the maximum relative error did not exceed 3.033%, indicating stable model performance even under less favourable conditions. Additionally, the maximum absolute error was below 0.65%, indicating low overall deviation.

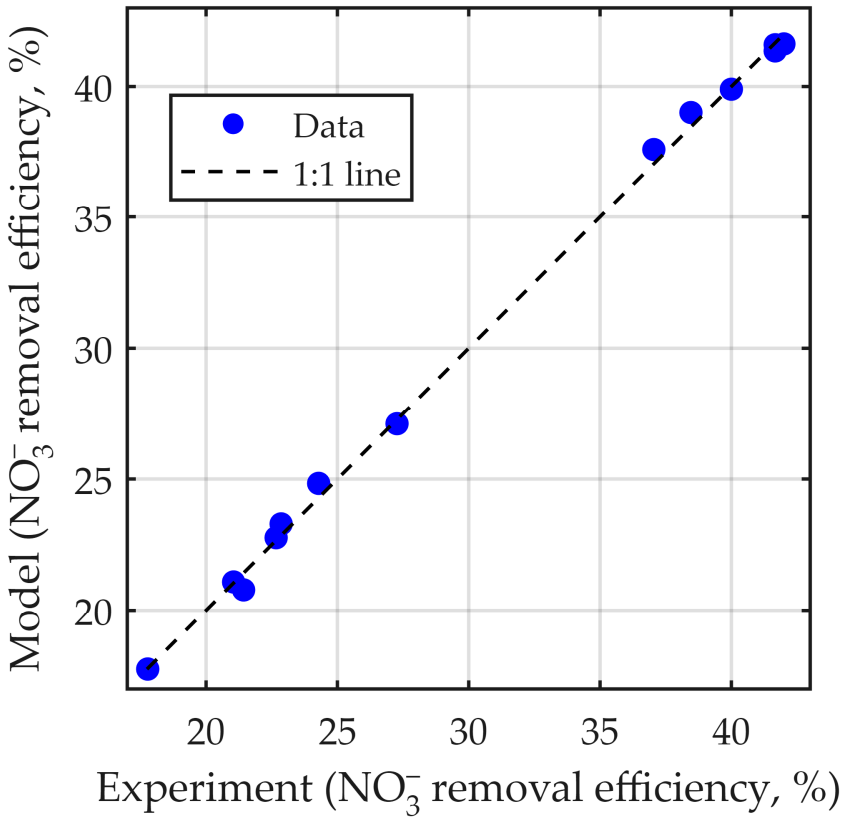

Figure 4. Parity plot of measured and simulated NO_3^- removal efficiency in the bioreactor.

Overall, these results confirm that the developed model provides reliable predictions of NO_3^- removal efficiency and is suitable for both process analysis and optimization applications.

Although the model demonstrates excellent agreement with the experimental dataset, it should be noted that the validation was performed using a limited set of representative field measurements covering the observed operational range. Therefore, the possibility of overfitting cannot be fully excluded. This limitation is further amplified by the relatively small size of the validation dataset, which covered a restricted range of operational conditions and may not fully represent the broader system variability. The inherent variability of biological and environmental denitrification processes introduces additional uncertainty that is not explicitly captured within the deterministic modelling framework. As a result, the reported performance should be interpreted as valid within the studied conditions rather than as fully generalizable across all operational scenarios.

During the parameter calibration process, a sensitivity analysis indicated that the temperature coefficient for denitrification (θ_N), the temperature coefficient under aerobic conditions (θ_O), and the maximum nitrate uptake rate during denitrification at 21 °C ($V_{N,21\,^\circ C}$ in mg L^{-1} h^{-1}) exhibited the strongest influence on simulated NO_3^- removal efficiency, and therefore required the most extensive refinement. In contrast, parame-

ters with lower influence on model outputs were retained at literature-based values to reduce parameter interdependencies and improve the stability of the calibration procedure. Due to the limited size of the available dataset, formal uncertainty propagation and cross-validation were not performed in the present study. These aspects are identified as important directions for future model development and validation and should focus on model evaluation using independent datasets and the incorporation of uncertainty quantification methods such as parameter confidence intervals and stochastic simulations to improve predictive robustness.

The analysis further revealed that the calibrated θ_N values could be associated with three distinct temperature regimes: below 6 °C, between 6 and 12 °C, and above 12 °C. In contrast, θ_O values could be classified into two regimes: below 12 °C and above 12 °C. At lower temperatures, reduced θ_O values were required to correctly reproduce oxygen consumption dynamics; otherwise, oxygen persistence in the system was overestimated by the model.

Experimental observations showed that the O_2 concentration in the influent water ranged from 3.25 to 4.4 mg L^{-1}, whereas within the bioreactor they decreased to 0–1.3 mg L^{-1} during measurement. In 32 out of the 59 measurements, oxygen was consumed completely, indicating the formation of strongly anoxic conditions favorable for denitrification. Among the 13 experiments selected for model validation, residual oxygen was detected in only two cases (0.05 mg L^{-1} and 1.3 mg L^{-1}), confirming that the model appropriately captures oxygen-limited conditions.

Based on the calibrated model parameters, two distinct temperature regimes were defined:

- For 6–12 °C:
  - Temperature coefficient for denitrification: $0.805 \leq \theta_N \leq 1.026$;
  - Temperature coefficient under aerobic conditions: $\theta_O = 1.02$;
  - Maximum NO_3^- uptake rate during denitrification at 21 °C: $19 \leq V_{N,21\,°C} \leq 35.8$ mg L^{-1} h^{-1}.
- For 14–19 °C:
  - Temperature coefficient for denitrification: $\theta_N = 1.15$;
  - Temperature coefficient under aerobic conditions: $\theta_O = 1.2$;
  - Maximum NO_3^- uptake rate during denitrification at 21 °C: $23.5 \leq V_{N,21°C} \leq 59$ mg L^{-1} h^{-1}.

These results indicate a clear temperature-dependent shift in both aerobic and anoxic process kinetics, with higher temperatures enhancing nitrate uptake rates and altering oxygen-related reaction dynamics.

The observed regime separation suggests that microbial activity exhibits non-linear temperature sensitivity, where low-temperature conditions are governed by enzymatic limitation, while higher temperatures shift the system toward substrate-controlled kinetics.

The dependence of θ_N and θ_O on inflow water temperature is presented in Figure 5. The observed trends confirm the strong temperature sensitivity of both denitrification and aerobic biochemical processes in the bioreactor system. These findings emphasize the importance of accurate temperature-dependent parameterization in predictive denitrification models.

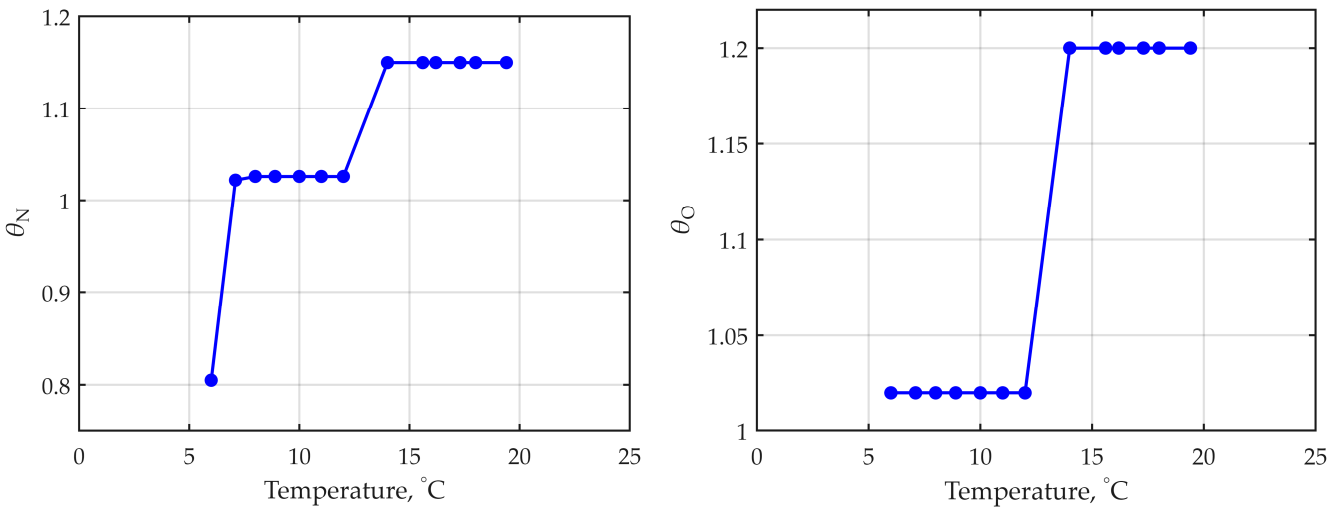

Figure 5. Dependence of the temperature coefficient for denitrification (**a**) and the temperature coefficient under aerobic conditions (**b**) on the inflow water temperature.

3.2. Influence of Bioreactor Length on Nitrate Removal Efficiency at Low Inflow Water Temperatures

A NO_3^- removal efficiency of approximately 40% is commonly considered a practical performance target for woodchip bioreactors under field conditions. Experimental observations indicate that this threshold is typically achieved within 1–5 h of hydraulic retention time under favorable conditions, with a carbon-to-nitrogen (C/N) ratio (defined as the ratio of carbon loss to nitrogen removal) ranging from 4 to 6 [20]. At elevated inflow temperatures (>20 °C), removal efficiency frequently exceeds 40%, whereas under low-temperature conditions this performance level is significantly more difficult to achieve, indicating the need for system optimization.

To quantify this effect, a representative low-temperature case was selected as a reference scenario. The bioreactor length was 100 cm, while width and depth were kept constant as described in the methodology. The influent NO_3^- concentration was 114 mg L^{-1}, decreasing to 90 mg L^{-1} after 2.33 h at +7.1 °C, corresponding to a removal efficiency of 21%, which is below the commonly targeted 40% performance level.

To investigate the role of reactor geometry, a scenario analysis was performed using different bioreactor lengths ($a = 50 - 250$ cm) under constant hydraulic conditions (flow rate = 1.4 cm h^{-1}). The model accurately reproduced the reference experimental case, confirming its predictive capability.

Simulation results (Figure 6) show that NO_3^- removal efficiency increases with bioreactor length due to extended hydraulic retention time and increased contact between drainage water and reactive woodchip media. However, the marginal gain decreases at longer lengths due to substrate depletion along the flow path, indicating a transition from kinetically controlled to substrate-limited conditions.

The relationship between bioreactor length and NO_3^- removal efficiency at +7.1 °C can be described by a cubic empirical function:

$$NO_3^- \text{ removal efficiency } (\%) = 2 \times 10^{-6} \cdot a^3 - 0.0019 \cdot a^2 + 0.4735 \cdot a - 9.5943 \quad (10)$$

here, a represents the bioreactor length (cm).

The high coefficient of determination ($R^2 = 0.9891$) indicates a strong goodness-of-fit, demonstrating that reactor performance can be reliably predicted as a function of bioreactor length under low-temperature conditions.

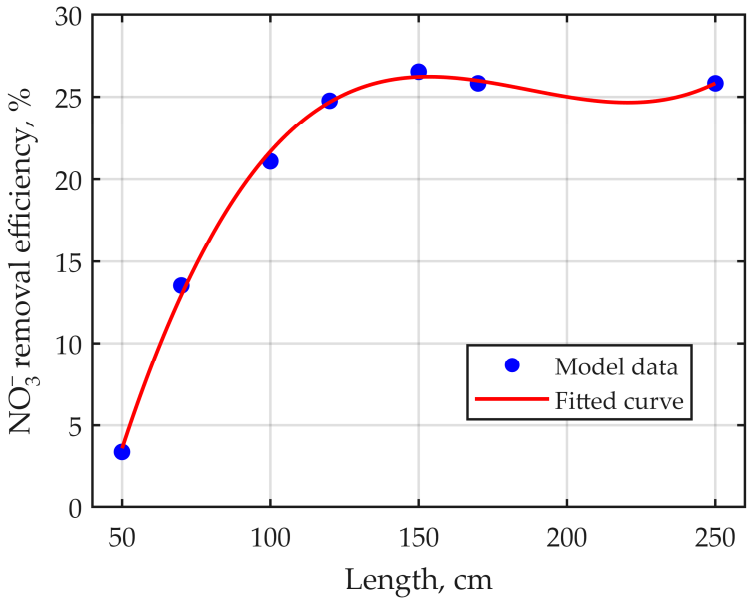

Figure 6. Dependence of NO_3^- removal efficiency on bioreactor length (inflow water temperature +7.1 °C.

A comparative simulation was also conducted at +15 °C under identical hydraulic conditions showed (Figure 7) consistently higher NO_3^- removal efficiency, confirming the accelerating effect of temperature on reaction kinetics rather than transport processes.

For the 15 °C case, the following empirical relationship was obtained:

$$NO_3^- \text{ removal efficiency } (\%) = 2 \times 10^{-6} \cdot a^3 - 0.001 \cdot a^2 + 0.1952 \cdot a + 32.827, \quad (11)$$

with $R^2 = 0.9964$.

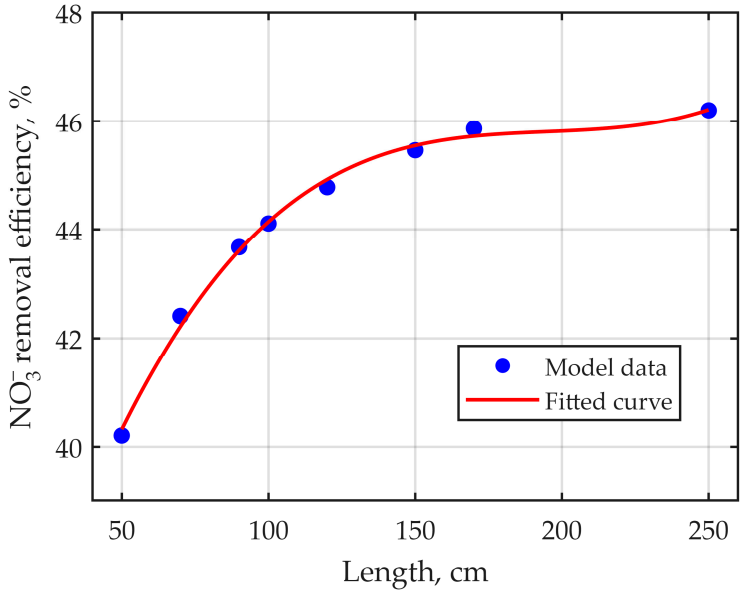

Figure 7. Dependence of NO_3^- removal efficiency vs. bioreactor length (inflow water temperature + 15 °C).

To extend the analysis toward design optimization, additional simulations were performed to identify conditions required to achieve a target NO_3^- removal efficiency of

40% across different temperatures. The results demonstrate that achieving this threshold depends on both bioreactor length and hydraulic loading, indicating coupled control of geometry and flow conditions.

At fixed bioreactor length of 50 cm and a water flow rate of 1.4 cm h^{-1}, the time required to reach 40% NO_3^- removal decreased with increasing temperature due to faster reaction kinetics. At 5 °C, 40% efficiency was reached after 5 h ($V_{N,21\,^\circ C} = 19$ mg L^{-1} h^{-1}), while at 10 °C and 15 °C lower $V_{N,21\,^\circ C}$ values (2.35 and 0.88 mg L^{-1} h^{-1}, respectively) were sufficient to achieve the same performance.

Further simulations indicated that in order to achieve 40% efficiency across different temperatures and bioreactor lengths, it is necessary to adjust not only the bioreactor length but also the water flow rate. This highlights that maintaining a consistent removal performance requires simultaneous consideration of both hydraulic conditions and temperature-dependent reaction kinetics.

Linear relationships between the water flow rate and the bioreactor length were observed:

$$\text{At } 5\,^\circ\text{C}: \; v = 0.0641\,a - 1.7534, \; \left(R^2 = 0.9991\right), \tag{12}$$

$$\text{At } 10\,^\circ\text{C}: \; v = 0.0501\,a - 1.0459, \; \left(R^2 = 0.9984\right), \tag{13}$$

$$\text{At } 15\,^\circ\text{C}: \; v = 0.0507\,a - 1.1818, \; \left(R^2 = 0.9958\right), \tag{14}$$

here, v represents the water flow rate (cm h^{-1}) and a is the bioreactor length (cm).

Overall, these relationships highlight the influence of temperature on hydraulic requirements: at lower temperatures, higher flow adjustments are needed to achieve the same NO_3^- removal efficiency, reflecting the slower kinetics of denitrification. Conversely, at higher inflow water temperatures, the flow adjustments are smaller due to accelerated reaction rates. This understanding provides practical guidance for scaling bioreactor dimensions and flow rates under varying environmental conditions while maintaining target NO_3^- removal efficiencies.

4. Discussion

A series of field pilot-scale experiments were conducted in a woodchip denitrification bioreactor to develop and validate a robust mathematical model describing nitrate (NO_3^-) removal in tile drainage water. The model, formulated as a system of nonlinear differential equations, enabled effective computer simulations of nitrate transport and transformation processes under varying temperature conditions. A numerical tool based on a finite difference scheme was implemented to solve the system of partial differential equations, allowing detailed analysis of NO_3^- removal performance along the bioreactor length.

The modelling results demonstrated a strong dependence of NO_3^- removal performance on bioreactor length and temperature. At a low inflow temperature of +7.1 °C, the relationship between reactor length and removal efficiency was well described by a cubic function (10), indicating a nonlinear increase in performance with increasing residence time. At elevated temperature (+15 °C), higher removal efficiencies were achieved under identical hydraulic conditions, confirming the accelerating effect of temperature on denitrification kinetics.

The results further show that achieving a target NO_3^- removal efficiency of approximately 40% requires coordinated adjustment of both kinetic and hydraulic parameters. Increasing the maximum nitrate uptake rate during denitrification significantly improves system performance under low-temperature conditions, although the required values decrease substantially as temperature increases. This confirms that temperature strongly governs microbial activity and reaction rates within woodchip bioreactors.

Alternatively, the same target efficiency can be achieved through hydraulic optimization. Simulation results indicate a clear dependence between flow rate and bioreactor length, suggesting that system performance can be maintained by balancing reactor geometry with hydraulic loading conditions. This relationship highlights the importance of considering both physical residence time and temperature-dependent reaction kinetics in design applications.

Overall, the combined experimental and modelling approach provides a comprehensive framework for understanding nitrate removal dynamics in woodchip bioreactors. The results demonstrate that reactor performance can be reliably optimized by integrating temperature effects with hydraulic and kinetic design parameters. This approach offers a predictive basis for improving the design and operation of denitrification systems in tile-drainage environments.

From a field-scale drainage system perspective, the results provide practical guidance for optimizing subsurface bioreactor design under varying climatic conditions. In particular, the identified relationships between temperature, hydraulic loading, and bioreactor length can be directly applied to improve nitrate attenuation in agricultural tile drainage networks. This supports the development of climate-resilient mitigation strategies for reducing nutrient export to receiving surface waters.

5. Conclusions

This study developed and validated temperature-dependent model for nitrate (NO_3^-) removal in a woodchip denitrification bioreactor treating agricultural tile drainage water. The model successfully reproduced field-scale observations and demonstrated strong predictive capability across varying hydraulic and thermal conditions.

The results confirm that nitrate removal performance is governed by the coupled effects of temperature, hydraulic retention time, and bioreactor geometry. Temperature was identified as the primary driver of reaction kinetics, while reactor length and flow conditions control contact time and overall treatment efficiency.

A key outcome of the study is that equivalent NO_3^- removal performance can be achieved through different combinations of temperature, bioreactor length, and hydraulic loading. This indicates a compensatory relationship between kinetic activity and system design parameters, which is essential for optimizing bioreactor performance under variable environmental conditions.

From an application perspective, the proposed model provides a practical tool for the design and optimization of woodchip bioreactors in agricultural drainage systems. The derived relationships between temperature, hydraulics, and reactor geometry can support improved system scaling and contribute to more efficient nitrate mitigation strategies in field conditions.

Author Contributions: Conceptualization, A.P. and F.I.; methodology, F.I. and J.D.-B.; software, J.D.-B.; validation, J.D.-B.; formal analysis, J.D.-B.; investigation, A.P.; resources, A.P.; data curation, A.P. and J.D.-B.; writing—original draft preparation, J.D.-B.; writing—review and editing, F.I., A.P. and J.D.-B.; visualization, J.D.-B.; supervision, A.P. and F.I.; project administration, A.P. All authors have read and agreed to the published version of the manuscript.

Funding: This research received no external funding.

Institutional Review Board Statement: Not applicable.

Data Availability Statement: Dataset available on request from the authors.

Conflicts of Interest: The authors declare no conflicts of interest.

References

1. Vismontienė, R.; Povilaitis, A. Effect of biochar amendment in woodchip denitrifying bioreactors for nitrate and phosphate removal in tile drainage flow. *Water* **2021**, *13*, 2883. [CrossRef]
2. Christianson, L.E.; Cooke, R.A.; Hay, C.H.; Helmers, M.J.; Feyereisen, G.W.; Ranaivoson, A.Z.; McMaine, J.T.; McDaniel, R.; Rosen, T.R.; Pluer, W.T.; et al. Effectiveness of denitrifying bioreactors on water pollutant reduction from agricultural areas. *Trans. ASABE* **2021**, *64*, 641–658. [CrossRef]
3. Schipper, L.A.; Robertson, W.D.; Gold, A.J.; Jaynes, D.B.; Cameron, S.C. Denitrifying bioreactors—An approach for reducing nitrate loads to receiving waters. *Ecol. Eng.* **2010**, *36*, 1532–1543. [CrossRef]
4. Addy, K.; Gold, A.J.; Christianson, L.E.; David, M.B.; Schipper, L.A.; Ratigan, N.A. Denitrifying bioreactors for nitrate removal: A meta-analysis. *J. Environ. Qual.* **2016**, *45*, 873–881. [CrossRef]
5. Zhang, Y.; Wang, L.; Han, W.; Wang, X.; Guo, Z.; Peng, F.; Yang, F.; Kong, M.; Gao, Y.; Chao, J.; et al. Nitrate removal, spatiotemporal communities of denitrifiers and the importance of their genetic potential for denitrification in novel denitrifying bioreactors. *Bioresour. Technol.* **2017**, *241*, 552–562. [CrossRef] [PubMed]
6. David, M.B.; Gentry, L.E.; Cooke, R.A.; Herbstritt, S.M. Temperature and substrate control woodchip bioreactor performance in reducing tile nitrate loads in east-central Illinois. *J. Environ. Qual.* **2015**, *45*, 822–829. [CrossRef]
7. Jéglot, A.; Audet, J.; Sørensen, S.R.; Schnorr, K.M.; Plauborg, F.; Elsgaard, L. Microbiome structure and function in woodchip bioreactors for nitrate removal in agricultural drainage water. *Front. Microbiol.* **2021**, *12*, 678448. [CrossRef]
8. Jaynes, D.B.; Kaspar, T.C.; Moorman, T.B.; Parkin, T.B. In situ bioreactors and deep drain-pipe installation to reduce nitrate losses in artificially drained fields. *J. Environ. Qual.* **2008**, *37*, 429–436. [CrossRef]
9. Lepine, C.; Christianson, L.E.; Sharrer, K.L.; Summerfelt, S.T. Optimizing hydraulic retention times in denitrifying woodchip bioreactors treating recirculating aquaculture system wastewater. *J. Environ. Qual.* **2015**, *45*, 813–821. [CrossRef] [PubMed]
10. Warneke, S.; Schipper, L.A.; Matiasek, M.G.; Scow, K.M.; Cameron, S.C.; Bruesewitz, D.A.; McDonald, I.R. Nitrate removal, communities of denitrifiers and adverse effects in different carbon substrates for use in denitrification beds. *Water Res.* **2011**, *45*, 5463–5475. [CrossRef]
11. Lee, S.; Cho, M.; Sadowsky, M.J.; Jang, J. Denitrifying woodchip bioreactors: A microbial solution for nitrate in agricultural wastewater—A review. *J. Microbiol.* **2023**, *61*, 791–805. [CrossRef] [PubMed]
12. Burbery, L.; Abraham, P.; Pearson, A.; Close, M.; Sarris, T. Design and performance characteristics of an in-stream woodchip denitrifying bioreactor for the treatment of agricultural drainage. 1. Design, hydraulics and nitrate removal. *Ecol. Eng.* **2025**, *219*, 107703. [CrossRef]
13. Burbery, L.; Abraham, P.; Pearson, A.; Sutton, R.; Weaver, L.; McGill, E.; Sarris, T. Design and performance of an in-stream woodchip denitrifying bioreactor treating agricultural drainage. 2. Co-benefits and greenhouse gas emissions. *Ecol. Eng.* **2025**, *219*, 107679. [CrossRef]
14. Bauwe, A.; Lennartz, B. Long-term performance of a denitrifying bioreactor for the treatment of nitrate-laden agricultural drainage water in northeastern Germany. *Ecol. Eng.* **2025**, *218*, 107675. [CrossRef]
15. Faramarzmanesh, S. Optimum hydraulic retention time, the best microbial community genus, and carbon sources in woodchip denitrifying bioreactors: A mini review. *Water Pract. Technol.* **2024**, *19*, 3495–3505. [CrossRef]
16. Moghaddam, R.; Christianson, L.E. Enhancing nitrate removal in denitrifying woodchip bioreactors: A comprehensive analysis of enhancement strategies and environmental trade-offs. *J. Water Process Eng.* **2025**, *78*, 108806. [CrossRef]
17. Halaburka, B.; LeFevre, G.H.; Luthy, R.G. Quantifying the temperature dependence of nitrate reduction in woodchip bioreactors: Experimental and modeled results with applied case-study. *Environ. Sci. Water Res. Technol.* **2019**, *5*, 782–797. [CrossRef]
18. Hassanpour, B.; Giri, S.; Pluer, W.; Steenhuis, T.S.; Geohring, L.D. Seasonal performance of denitrifying bioreactors in the Northeastern United States: Field trials. *J. Environ. Manag.* **2017**, *202*, 242–253. [CrossRef]
19. Hoover, N.L.; Bhandari, A.; Soupir, M.L. Woodchip denitrification bioreactors: Impact of temperature and hydraulic retention time on nitrate removal. *J. Environ. Qual.* **2015**, *45*, 803–812. [CrossRef]
20. Povilaitis, A.; Matikienė, J.; Vismontienė, R. Effects of three types of amendments in woodchip-denitrifying bioreactors for tile drainage water treatment. *Ecol. Eng.* **2020**, *158*, 106054. [CrossRef]
21. Nečiporenko, A. *Mathematical Modeling of Bioreactor Control*; Vilniaus Universiteto Leidykla: Vilnius, Lithuania, 2021. [CrossRef]
22. Halaburka, B.; LeFevre, G.H.; Luthy, R.G. Evaluation of mechanistic models for nitrate removal in woodchip bioreactors. *Environ. Sci. Technol.* **2017**, *51*, 5156–5164. [CrossRef] [PubMed]
23. Baronas, R.; Ivanauskas, F.; Kulys, J. *Mathematical Modeling of Biosensors*; Springer: Cham, Switzerland, 2021. [CrossRef]